Light Scattering Simulations using Complex Subsurface Models

Morgan Schramm*, Jay Gondek*, and Gary Meyer
Dept. of Computer and Information Science
University of Oregon
Eugene, Oregon 97403

Abstract

New techniques are presented for simulating complex surface reflection phenomena. The approach involves the modeling of surface and subsurface microstructures, the simulation of how light interacts with this geometry, and the recording of the scattered light as a bidirectional reflection distribution function. Previous light simulation techniques employed in this method are extended to include subsurface refraction and multilayer interference effects. A complicated modeling and simulation example is presented that involves the structure of a hummingbird feather and multilayer interference. Light reflection measurements are recorded from paper samples, and a second modeling and simulation exercise is undertaken in an attempt to reproduce the measured results. In both cases, first order agreement is achieved between the simulations, the available analytical models, and the measured data.

Keywords: BRDF, local illumination modeling, multilayer interference, reflectance measurement, surface modeling.

1 Introduction

Computer graphic techniques that were developed to simulate light reflection in large scale environments have recently been applied to the modeling of light interactions at much smaller scales. In the traditional approach to computer graphics, large objects such as a table and chair are modeled and then placed in a room containing light sources. Each of the objects in the environment is assigned surface reflection properties, and a global illumination model is used to produce a picture of the scene from a specific viewing direction. The application of these techniques to much smaller scales begins with the modeling of a minute portion of an object's surface. The microstructures above and below this surface are defined and a narrow beam of light is directed at the material. A technique such as ray tracing is used to model the interaction of the light with both the surface and subsurface. The simulation is repeated for other incident directions and the resulting bidirectional reflection function (BRDF) is recorded. This BRDF can be assigned as a surface reflection property when simulating large scale environments.

There are a number of advantages to using simulation techniques to create new surface reflection properties. The current analytically defined local reflection models used in computer graphics have limited capabilities. While much effort has been put into refining the specular term in these models, little has been done to better characterize the diffuse term. It is also difficult to use these models when the surfaces exhibit anisotropic reflections and interference effects. In many cases it is also not clear what values to assign to the free parameters in the model in order to match specific reflection results. The simulation of surface reflection phenomena also has application beyond the field of computer graphics. For example, the simulation tool, when it is fully developed, could be used in the paint and coatings industries to explore the reflection properties of proposed new materials before they are actually fabricated.

This paper extends, in three important ways, the use of computer graphic techniques to model light reflection at very small scales. First of all, in Section 3, the range of optical phenomena that have previously been included in such simulations is increased. The index of refraction is allowed to vary with wavelength and the resulting effects are modeled. In addition, the problems inherent in simulating multilayer thin film interference are addressed. Secondly, in Section 4, modeling techniques are developed to deal with complicated subsurface microstructures. The example

* Current Address: Hewlett Packard Company, PO Box 8906, Vancouver WA, 98688-8906

chosen is the hummingbird feather. Finally, in Section 5, an attempt is made, using paper as the test material, to actually "close the loop" and compare simulated results with measured data. This makes it possible to use these techniques to answer some real world questions about reflection.

2 Background

Much of the previous local illumination work has focused on component-based analytical reflectance models (Bui-Tong, 1975, Blinn, 1977, Cook and Torrance, 1982, He et al., 1991). Some of these models are computed using physically based parameters; however, these models inherently lack the generality necessary to simulate arbitrary surface light scattering functions. The most general method of describing light scattering phenomena is provided by the bidirectional reflectance distribution function (Kajiya, 1986). A BRDF relates the ratio of reflected radiance to incident flux density for all angles both in the incidence and exitance directions. In addition, these ratios should be separately available across the entire spectrum of visible light in order to accurately represent the reflectance properties of surfaces whose spatial and spectral scattering characteristics are interrelated. For example, the specular composition of light scattered from surfaces such as thin films is directly related to the spatial geometry of the illumination and viewing conditions.

Cabral et al. (1987) used a BRDF to represent the scattering function of the light reflected from an explicit surface model. In this approach an array of triangular microfacets was used to represent a surface and a reflectance function was then computed by considering the self-shadowing and masking effects that a beam of light covering a significant area of this surface would be subject to. The resulting reflectance distribution is captured in a hemisphere which has been discretely divided into a number of cells and positioned atop the surface. A spherical harmonic representation of the BRDF is computed from the reflectance values of these cells. Research done by Westin et al. (1992) extended the work of Cabral with more elaborate surface representations and a method that allowed the direct computation of the spherical harmonic function during a ray casting simulation. Westin used this new approach to produce realistic reflectance functions for anisotropic surfaces such as brushed aluminum and textiles.

The spherical harmonics representation of the BRDF is useful for characterizing the entire spatial distribution of the light scattered from a surface. However, it does not contain a provision for the spectral component of this scattering. A separate spherical harmonic function must be used for each wavelength in order to capture the spectral aspect of the scattering from a surface. This hinders the efficiency of the representation and complicates its calculation. A BRDF representation presented by Gondek, Meyer, and Newman (1994) addresses this issue. This representation integrated the spectral and spatial characteristics of the BRDF in a single data structure which was then used in a Monte Carlo raytracer to generate realistic images of complex surfaces, including pigmented plastic, thin-films, and interference paint. The software developed for these simulations was described as a virtual goniospectrophotometer. An actual goniospectrophotometer is a device which is used to measure the spectral and spatial scattering of light from a surface.

To generate reflectance functions with the virtual goniospectrophotometer, numerous simulated light rays are shot into a surface model from a range of incident directions. The modeled surface can be composed of various opaque and transmissive geometric primitives and tessellated height fields. Polarization, phase, and amplitude are computed for individual rays as they propagate through the model. These optical characteristics are affected by absorption, material interfaces, and geometric distances. Tracking polarization, phase, and amplitude allows the model to be used for computing complex sub-surface scattering events, such as the reflectance from interference pigments.

The scattering that results from the interactions of these multiple rays with the surface model is captured by a novel data structure which is tailored for this type of simulation. A geodesic sphere is used to represent the exiting directions above and below the surface, with each facet of this sphere designed to capture the exiting rays over a discrete range of possible exit directions. The sphere dynamically subdivides during the course of the simulation so that regions containing high degrees of variation are more finely discretized than more uniform regions. The rays captured in each facet of the dome are then used to calculate and store the spectral reflectance ratio with respect to the incident direction. This ratio represents the spectral reflectance for the range of exit angles that the facet covers. Spectral transmitance ratios are similarly created by capturing the rays exiting the bottom of the model. From the discrete incident sample directions, ratios for a given arbitrary incident angle are generated by interpolating the ratios across the four nearest discrete angles which were sampled in the simulation. This data is used to represent the BRDF of the modeled surface in a Monte Carlo raytracer which enables synthetic images of these surfaces to be generated.

3 Optics Model Extensions

The original optics model described in Gondek et al. included wavelength dependent amplitude, phase, and polarization. By tracking and computing these physical optics characteristics, it was possible to model the reflection from structures that produce interference through thin-film mechanisms. The optics model used in the virtual goniospectrophotometer has been extended in two important ways to allow for the synthesis of a larger class of light scattering phenomena. Functionality added to the optics model includes a multilayer thin film solver which overcomes the computational problems associated with ray-casting through many dielectric thin-film layers. In addition, another optics mode was added in which a single ray is cast for each wavelength of light to allow wavelength-dependent refraction effects.

When simulating light rays incident upon a thin film system with many layers, each layer gives rise to a number of reflected and transmitted rays. The total number of rays that propagate through the system are exponential with the number of film layers, making sampling by traditional ray casting impractical. One solution to this problem is to use ray casting to determine where multilayer structures exist. Once a multilayer film is discovered, an analytical solver is employed to determine the reflectance and transmittance of the film. This solution is then brought back into the ray casting system and used to properly modify the fields of the reflected and transmitted rays from both sides of the multilayer structure.

To implement this strategy, a multilayer finding algorithm is employed each time a ray strikes a dielectric surface. The multilayer finder proceeds to cast transmitted rays and notes the path lengths, incident angles, and indices of refraction for each additional layer that is found. The finder terminates when it casts a transmitted ray that either strikes a non-dielectric, or strikes a surface that has a normal that is different, to within a small tolerance, from the normals of the previous layers. If a multilayer is discovered, an analytical multilayer solver is called with the data that was collected by the finder. The solver computes the correct reflected and transmitted fields, and returns these results back to the ray casting software. The fields that result from multilayer interference can efficiently be computed using dynamic programming techniques (for example, see Aho et al., 1972).

The multilayer solver works by successively replacing three-layer systems with two-layer systems, or similarly, one may think of the solution as reducing two-interface systems to one-interface systems. This is

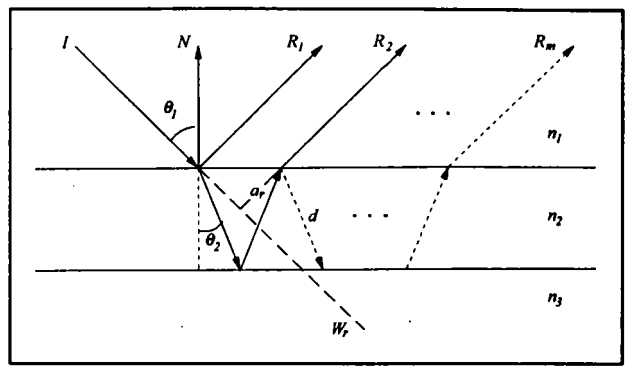

Figure 1: Reflectance geometry of three-layer film

accomplished by computing the reflectance and transmittance characteristics of the two-interface system, and then replacing both interfaces with a single interface that simulates those characteristics. For a stack of films where there are more than two interfaces, the algorithm simply proceeds from the top down, collapsing the intermediate layers one at a time until a single interface remains. The reflectance and transmittance from the final interface is the solution to the problem. The computation time associated with this algorithm grows linearly with the number of film layers, and thus this method provides an efficient solution to the exponential explosion of ray intersections needed to characterize a multilayer film system. Similar methods for computing the reflectance and transmittance of multilayer systems have been used in the field of optics (for example, see Heavens, 1955).

The multilayer solver will be described in terms of a single plane of polarization for light incident upon a two-interface system. The solution for the orthogonal plane of polarization is similar. Fresnel's equations give amplitude coefficients for the reflected and transmitted rays from light incident upon a dielectric boundary (Hecht 1987). These equations are used to compute the amplitude coefficients that result from multiple reflections within the two-interface system.

Figures 1 and 2 show the geometry of a two-interface system. In these figures, n_1, n_2, and n_3 are the three indices of refraction, $R_1 \ldots R_m$ are the reflected rays, and $T_1 \ldots T_m$ are the transmitted rays. For the particular incident angles of light upon each interface, Fresnel's equations give the reflected and transmitted amplitudes denoted by r_{12}, t_{12}, r_{23}, t_{23}, r_{21}, and t_{21} for boundaries $n_1{:}n_2$, $n_2{:}n_3$, and $n_2{:}n_1$, respectively. The m amplitude coefficients for reflected rays that result from multiple bounces are given by

$$R_{1,A} = r_{12}$$

$$R_{2,A} = t_{12} r_{23} t_{21}$$

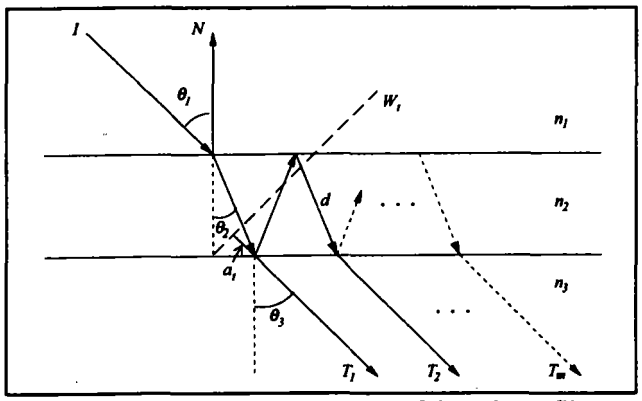

Figure 2: Transmittance geometry of three-layer film

and in general, for $m > 2$,

$$R_{m,A} = t_{12}(r_{23}r_{21})^{m-2} r_{23} t_{21}.$$

Similarly, the amplitude coefficients for the transmitted rays are given by

$$T_{1,A} = t_{12}t_{23}$$

and in general, for $m > 1$,

$$T_{m,A} = t_{12}(r_{23}r_{21})^{m-1} t_{23}.$$

These amplitude coefficients are used in conjunction with phase information for each ray to compute the final reflected and transmitted fields.

It is necessary to compute phase changes for the exiting rays in order to account for interference effects. This is done by setting the phase of the incident ray to 0 and computing the phases of the exiting rays based on optical path lengths. To determine these phase differences, the optical path lengths must be computed to a wavefront that is orthogonal to the direction of propagation. The specific position of the wavefronts used in the calculations are shown as W_r and W_t, in Figures 1 and 2. These wavefront positions are important because, as previously mentioned, the two-interface system is reduced to a single interface. When a ray strikes the single interface, the reflected and transmitted rays originate from the point of incidence. Therefore, the change in phase that the reduced interface imparts upon the ray must correspond to a wavefront originating at the point of incidence. With respect to the wavefront W_r, the optical path lengths for the reflected rays are

$$R_{m,P} = (m-1)(2dn_2 - a_r n_1)$$

where

$$a_r = 2d \sin\theta_2 \sin\theta_1.$$

Similarly, the optical path lengths for the transmitted rays with respect to wavefront W_t are

$$T_{m,P} = (2m-1)(dn_2 - a_t n_3)$$

where

$$a_t = d \sin\theta_2 \sin\theta_3.$$

Finally, the fields of each of the reflected and transmitted rays are summed by wavelength to produce a single reflected and transmitted field at each wavelength. The resulting fields give the change in amplitude and phase for light incident upon this system. The data is used for further reduction of a multilayer by replacing the two-interface system with the single interface. During later computations when rays strike this interface, the computed amplitude changes are used instead of Fresnel's coefficients to predict change in amplitude of incident rays, and phase change is accounted for by adding the pre-computed phase change to the phase of each ray incident upon the reduced interface. Note that a two-interface system can only be replaced by a one-interface system by computing the resulting reflected and transmitted fields for rays incident from both the n_1 medium and the n_3 medium. This solution is needed because further computations may simulate rays incident upon either side of the interface.

The hybrid optics model that combines ray sampling and the multilayer thin film solver enables the simulation and investigation of reflectance functions from complicated structures. As a first application of the multilayer solver, an ideal model of the interference structure for the Morpho butterfly was created by simply stacking alternating high index films separated by air. These films were assigned an index of refraction of 1.53 to match that of the Morpho (Anderson and Richards, 1942), and the thicknesses were taken to be 50 *nm* for the high index films, and 150 *nm* for the air gaps between the films. Figure 3 shows the results of the simulation for the described multilayer configuration with an increasing number of layers. The Morpho butterfly has twelve mullions on each scale, so the image for the twelve high-index layer film (bottom, right of Figure 3) most closely corresponds to the reflectance from the actual butterfly. It should be noted that this is a large simplification of the structure on the wing of the Morpho; the mullions and air spacings have some variance in their thicknesses, and more importantly, the structure on the Morpho appears to be anisotropic due to the directional arrangement of the scales. Section 4 provides a description of more advanced modeling techniques. An analytical formula for the reflectance from this configuration was used by Smits and Meyer (1991) to produce the iridescent colors of the Morpho butterfly in a computer generated image.

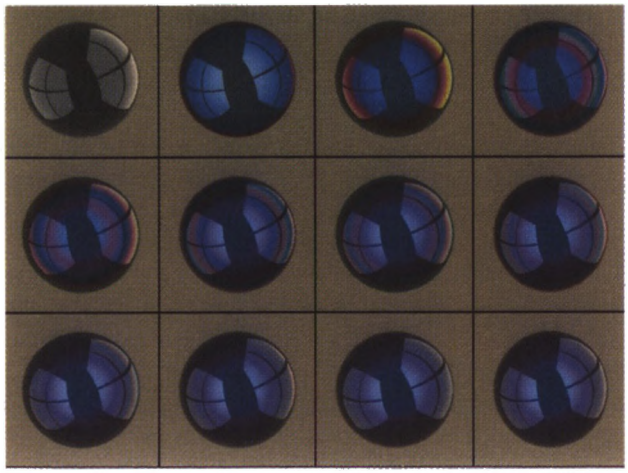

Figure 3: Computer generated example of multilayer interference for stacks of one to twelve high index films

In addition to the multilayer solver, the original Gondek et al. optics model was also extended to synthesize wavelength-dependent refraction effects. This was done by simply assigning a field representing a single wavelength to each ray cast at the surface model, and casting enough rays to sufficiently sample the spectrum of visible light. Refraction effects are computed during the simulation by assigning wavelength based refraction tables for each object in the model. An example structure that demonstrates the effect of wavelength dependent refraction is the Christiansen filter, a spectral filter that was used for early optical applications such as spectroscopy (Evans, 1948; McAlister, 1935; Rayleigh, 1885). This filter is unique because it relies upon optical dispersion to produce a narrow-band light filter. Construction of the filter is accomplished by immersing finely ground glass particles in a transparent medium, where the wavelength dependent index of refraction for the glass and the medium share the same value at a specific wavelength, and are different at all other wavelengths. For the wavelength where the indices are the same, light passes through the filter with virtually no internal scattering. As the difference between the indices of the two dielectrics increases for different wavelengths, more scattering occurs. The result is a nearly perfect transmission of certain wavelengths of light, and a diffuse scattering of the complementary color. Lord Rayleigh (1885) pointed out the fact that diffuse illumination of the filter produces little visible color due to the mixing of complementary colors; directional lighting is required to properly view the phenomena.

A Christiansen filter was simulated by suspending approximately 14,000 microspheres in a matrix, where the indices of refraction for the particles and matrix are

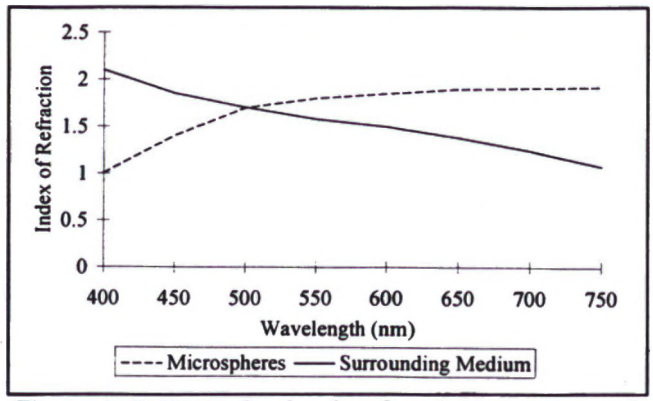

Figure 4: Indices of refraction for glass particles and surrounding substrate for a Christiansen filter

given in Figure 4. Rays representing twenty unique wavelengths of light were cast at this model to record the dispersion that occurs within this system. Figure 5 shows a computer generated scene where the measured scattering function for the Christiansen filter has been applied to a square spectrophotometer cell. The left half of this figure shows the transmission characteristics of the filter from bright light propagating from an area light source, through a window into a dim room. Note the green appearance of the directly transmitted light, which corresponds to the wavelength where the curves in Figure 4 cross. The diffusely transmitted light corresponds to a mixture of the wavelengths near the 500 *nm* position. The more the indices vary for a given wavelength, the more scattering occurs. The greatest difference in the indices of refraction for this example occur at the red and blue regions of the visible spectrum. At these wavelengths, the scattering is so prolific that much of the incident light is not transmitted through the filter; instead, this light is scattered back toward the incident side. This effect is visible in Figure 5 (right) where the viewpoint is now positioned outside the dim

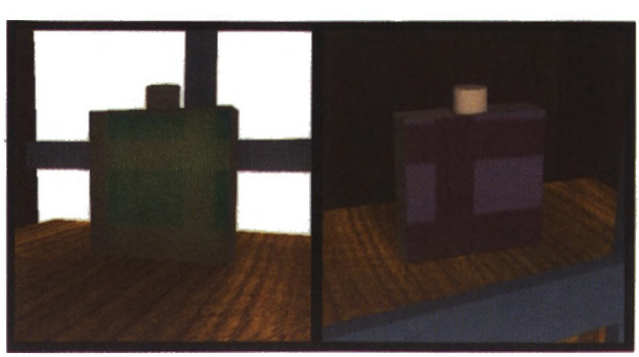

Figure 5: Computer generated images showing the transmitted and reflected scattering of light from a simulated Christiansen filter.

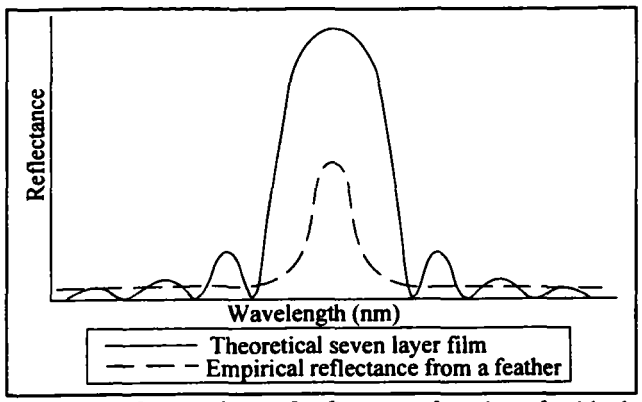

Figure 6: Comparison of reflectance functions for ideal thin films and an iridescent hummingbird feather. (From Greenwalt, 1960)

room, and the line of site is directed through the window, at the filter. The vivid magenta diffuse reflectance is due to the mixing of the scattered red and blue wavelengths of incident light. Thus the Christiansen filter provides an interesting light scattering function where the observed color from the filter is dependent on the spatial distribution of the observed reflectance. Note that the simulated glass particles and suspending matrix used to create the filter were completely transparent; it is the dispersion of light that imparts the specific colors upon the filter shown in Figure 5.

4 Advanced Modeling

In this section, subsurface modeling techniques are employed to explore the surface reflectance properties of an iridescent hummingbird feather. Previous studies have used a variety of elementary geometries to represent subsurfaces at the microscopic level in order to simulate local reflectance functions (Hanrahan and Krueger 1993, Gondek et al. 1995, and Dorsey and Hanrahan 1996). By developing detailed morphologic models of an animal structure, it is shown how the virtual goniospectrophotometer can be used to analyze structures which approach the complexity of those that have been observed in nature. The iridescent colors found in certain hummingbirds are, like that of the Morpho butterfly described previously, structural in nature. Since these birds have been studied by ornithologists, biologists, and optical scientist alike, the results of their studies can be used as a basis from which a model of these iridescent feather surfaces can be developed. These models also present a more robust case for the multilayer solver described in the previous section.

An electron microscopy study performed in 1960 by Greenwalt, Brandt, and Friel established that the iridescent color found in some hummingbirds is most likely the result of multiple stacks of thin film-like structures embedded in their feathers. Although the observed reflectance functions for these feathers show similarities to ideal thin films, there existed some anomalies that were attributed to structural deviations from ideal thin films. The iridescent feather barbules were found to contain multiple layers of thin platelets stacked in a very regular pattern. These flattened, elliptically shaped plates were composed of melanin, which has a high index of refraction. Platelets located in the iridescent sections of the feather also had foam-like air pockets in their center. Mosaics of these platelets were distributed in evenly spaced layers embedded in karatin, a low index material.

The dimensions and periodic nature of this structure suggests that thin film interference is possible. However comparisons of the theoretical curves for ideal thin films to those observed in the iridescent feathers revealed some anomalies. An example comparison is shown in Figure 6. The theoretical curve of an ideal seven layer stack of alternating high and low index of refraction materials is shown along with the empirical reflectance curve of the iridescent feather from a Red Gorget hummingbird. This feather was found to have seven layers of platelets of similar dimensions to those of the thin films represented in the ideal case. These curves show that there are no secondary peaks in the empirical case. Greenwalt attributes this absence to "surface fluctuations in the platelets".

A second discrepancy between the two curves is the sharper peak exhibited in the empirical case. To account for this, Greenwalt developed a theoretical model for interference of optically *non-homogenous* materials. It was argued that the structurally reinforced air pockets in the platelets caused a transitional increase in the index of refraction as a function of the distance along the z axis from the center of the plate. In this way, the index of refraction of the platelets could be represented by a smoothly varying function which could then be integrated over the thickness of the platelets. By using methods of differential calculus the authors were able to generate approximate analytical solutions for this model of the platelets that better agreed with the empirical curves. Their solution involves replacing the non-homogenous portions of the platelets, namely the center air pockets, with a homogenous mass that has the effective refractive index calculated by integrating over the non-homogenous areas. While their new analytical solution was much closer in shape to the empirical results, the issue of the absence of secondary peaks remained unresolved.

Three models of an iridescent Calypte Anna, or Green Gorget hummingbird feather, were developed for use in the virtual goniospectrophotometer. The surface reflectance functions that were generated from these simulations were then compared with those of the Greenwalt theory. By adopting an approach that progressively refined the model in order to more accurately represent the microgeometry of the feather, surface reflectance functions were generated with similar characteristics to those found in the study. The stages of this refinement included modeling the feather successively as a collection of ideal thin films, a stack of broad rectangular plates and an array of interlocking bricks.

While the theoretical solutions of Greenwalt were not used directly in these simulations, one of their techniques was used to simplify the model. Instead of developing a model of the platelets in which the internal air pockets are explicitly included, they were replaced with uniform sub-regions of the same optical thickness reported in their study. Even with the multi-layer detection algorithm, the running time of the simulations would have been unreasonably long without this simplification.

The first approximation to the feather structure was constructed with simple thin films similar to those used in the modeling of the Morpho butterfly. 14 layers of alternating high and low refractive materials were used to represent the seven layers of platelets in a Green Gorget feather. The high refractive layers, which were meant to represent the melanin body of the platelets, were given an index of 2.0, and the low refractive layers, which represented the air pockets, were assigned an index of 1.50 in accordance with the values found by Greenwalt. The high index layers were 148 *nm* thick, except for the first and last layers which were half that, or 74 *nm* thick. The low index layers all had a thickness of 98 *nm*. These values correspond to the mean dimensions reported in the study. As expected, this model produced reflectance functions which were identical to a multi-thin film system and included a broad specular peak similar to that of the theoretical curve in figure 6.

An intermediate stage of refinement involved replacing the ideal thin films with broad high index boxes embedded with low index centers. By incorporating geometric primitives rather than thin films, we were able to confirm that the multi-layer algorithm would function properly with more complicated models. These broad plates were 172 *nm* thick and contained rectangular cores with a 98 *nm* thickness. The identical indices of refraction used in the thin film case were used here, and the simulation results produced matching

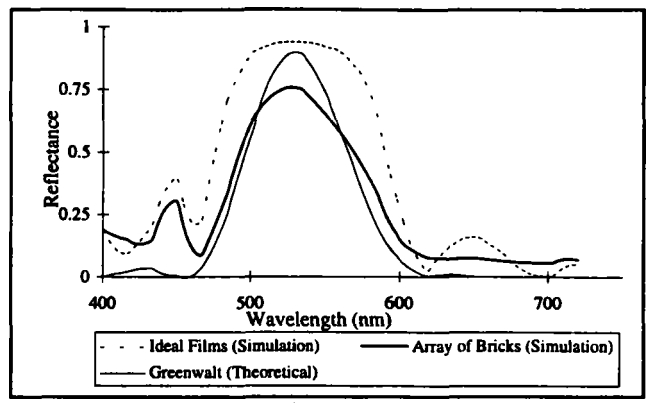

Figure 7: Comparison of reflectance functions for array of bricks model.

reflectance functions to those obtained by the previous thin film model.

Neither of the models up to this point had represented the individual platelets found in the feather. All the platelets on one level were represented only as a conglomerate film or box. By further refining the model to include the individual platelets, reflectance functions with better correlation to those observed in Greenwalt's study were generated. Each of the broad plates of the previous model were broken into an array of interlocking bricks. Seven layers of these bricks were used, corresponding to the seven layers of platelets. The horizontal dimensions of the bricks were set equal to the average dimensions of the platelets as reported in the study: 1500 *nm* by 2000 *nm*. The thickness of the bricks and their low index core were also the same as the previous model. The reflectance functions generated by the simulations are shown in Figure 7. This reflectance function shows similar characteristics to the one generated by the Greenwalt theory. The bandwidth of the primary peak has narrowed and the secondary peaks, while still visible, have been attenuated. The inclusion of the explicit modeling of the platelets in this case resulted in better agreement.

By developing the geometric model beyond simple ideal thin films, the reflectance functions generated by the brick model begins to show some of same characteristics that distinguish Greenwalt's results from that predicted by ideal thin films. While the array of bricks models the mosaic-like structure of the feathers platelets, focusing on a better representation of the individual platelets and their spatial relationships would further refine this model and improve the resulting reflectance functions.

5 Measurement vs. Simulation

In turning our attention to the next surface to be analyzed, paper, note that all the cases reviewed up to

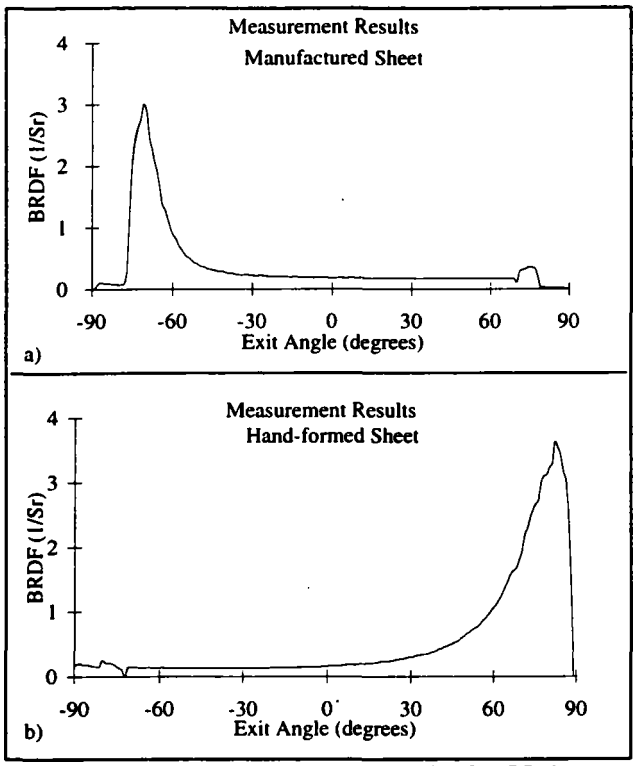

Figure 8a and 8b: Measurement results for 75 degrees incident illumination on the Manufactured and -75 degrees on the Hand-formed sheets.

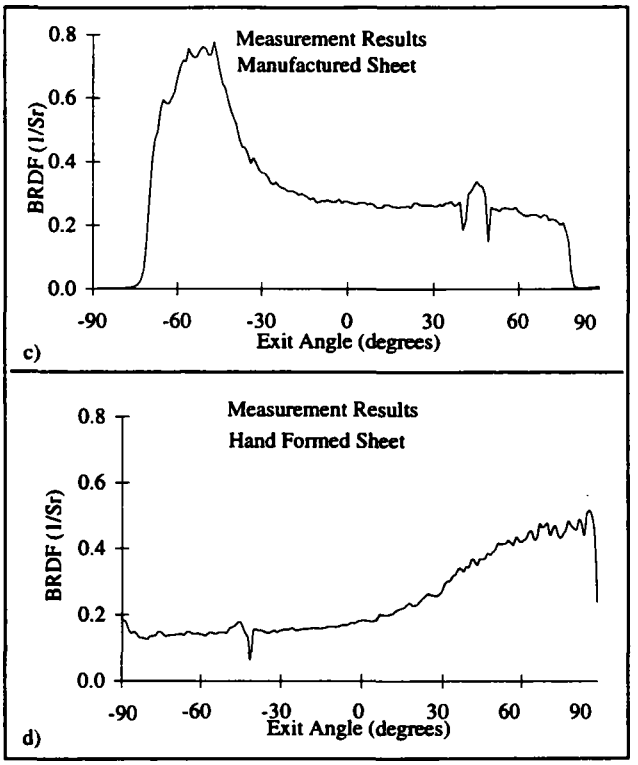

Figure 8c and 8d: Measurement results for 45 and -45 degree incident illumination.

this point have compared simulation results to results predicted by either established theories or previous optical studies. For this exploration, measurements of the surfaces in question were actually produced for purposes of comparison. Two specific phenomena were concentrated on: anisotropic reflectance functions caused by fiber orientation, and reflectance in the incident direction (backscatter). Specific paper samples were chosen and optical measurements were performed upon them in order to characterize these effects. Models were then constructed for use in the goniospectrophotometer in an attempt to reproduce these effects. Insight into the mechanics of the these optical effects is gained by comparing the measurement results with those obtained by simulations.

Two different types of paper were chosen for this study. The first sample was machine manufactured, and had a smooth, white, somewhat glossy appearance. This paper was coated with a clay and calcium carbonate mixture and it was hypothesized that the morphology of these coating materials was responsible for some of the observed retro-reflectance found in this sheet. Additionally, it was also predicted that this sample would display anisotropies in it's measured reflectance functions, since it was machine manufactured and it's underlying fiber web has an orientational preference. The second specimen was typical of heavy writing grade bond. This sample was more roughly textured than the previous, slightly yellow in hue, and diffuse in appearance. This sheet was hand formed and did not contain any secondary materials thus providing a number of benefits for this study. Since it was composed only of pulp it was easier to accurately model than the previous specimen. It would also provide us with an opportunity to confirm our speculation regarding the role of coatings in the backscatter phenomenon since this sheet was uncoated.

5.1 Paper Measurements

The optical profiling was performed by a third party laboratory and involved measuring the light scattered from the samples when illuminated by a laser. The Schmitt Measurement Systems CASI Scatterometer uses a 670 *nm* laser in an (S)-polarization state that was arranged so that the incident beam was at a specified angle with the normal of the specimen. Measurements were then taken by recording the magnitude of the reflected light at discrete locations on the hemi-circle perpendicular to the horizontal plane of the specimen that is formed by sweeping out the angles from -90° to ~+80° with respect to the normal. This type of meas-

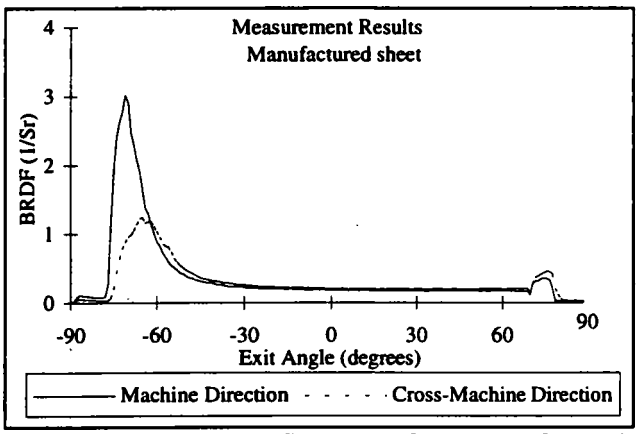

Figure 9: Measured reflectance of the manufactured sheet with the illumination parallel to both the cross- and machine directions. Incident illumination is at 75°.

urement sweep was performed for a family of incident angles on each specimen. A similar experimental method was employed in the 1991 Letteri et al. study of light scattering from glossy coated papers. For the purposes of the current study, measurements were also taken with the specimens rotated 90° in the horizontal plane, in order to record any anisotropies in the reflectance functions. Reflectance functions for two incident angles on the both samples are shown in Figure 8.

When paper is formed by machine, fibers are deposited on a moving screen and will tend to align themselves parallel to the direction the screen is moving. The direction of this orientation is called the *grain* or *machine* direction, and its effects on various mechanical properties are well documented. However, no research has been done regarding the optical consequences this alignment tendency might have. There is reason to believe that fiber orientation introduces anisotropy in the optical properties of the sheet similar to those encountered in the mechanical properties. Because of the geometry of the fibers in the web, incident light that is parallel to the machine direction should reflect light in a more specular fashion than identical light incident in the cross direction. This phenomenon would manifest itself only in a full spatial profile of the reflected light.

Separate measurements were taken on the machine manufactured sample for incident illumination parallel to both the machine and non-machine directions. The resulting reflectance functions show a greater specular peak for light incident along the machine direction than for identical illumination in the cross direction. This confirmed that anisotropy exists in the reflectance functions for this sheet. Figure 9 clearly shows this effect for 75° incident illumination.

One unexpected result from the initial set of measurements was the significant backscatter, or retroreflection for the manufactured sheet. There is a noticeable rise in the reflectance curves around the retroreflection angle in all cases and, for 20° incident (not shown), the measured backscatter is actually of the same magnitude as the specular reflection. (The discontinuities in the curves at the edges of these back scatter peaks are an artifact of the laboratory's experimental set up.) The decision to focus on this issue was made only after detecting this feature in the initial measurements.

5.2 Paper Models

In order to reproduce the anisotropic effect in simulations, models of the paper's fiber web were produced. The web of a sheet is composed of a collection of slender transparent fibers which resemble hollow cylinders and are oriented somewhat randomly in the horizontal plane of the sheet. Concentric cylinders were used to represent a fiber for our model. The space between the two cylinders represents the fiber while the interior cylinder represents the hollow core. In the pulping and web formation process, fibers may undergo deformations and come to resemble thin ribbons. Studies have shown that fibers will generally deform in predictable ways according to such factors as the fiber source, pulping technique, and method of construction (Jayme and Hunger 62, Wrist 67). For the purposes of this study, a simple deformation that compressed the fibers in one direction perpendicular to their long axis was chosen. The dimensions of our cylinders were set to be 2 *mm* long, .02 *mm* in diameter for the outer cylinder, and 0.01 *mm* diameter for the inner cylinder. These numbers correspond to the dimensions of typical wood pulp fibers (Dodsen and Fekih 91).

These fibers were used to construct three models of a sheet section. The first "fully oriented" sheet consisted of a stack of ten layers of fibers. Each layer consisted of ten fibers placed side by side and oriented parallel to the machine axis. Using the same number of fibers as the fully oriented sheet, a semi-random web was also constructed so that the fibers would have a mean angular variance of 15° from the machine direction. Finally, a fully random web was also created which represented a sheet with no machine induced directionality. In order to simplify the construction of the random sheets, they were allowed to grow unconstrained in the z direction which allowed for a denser horizontal packing, but produced models that did not correspond to the z dimensions of actual sheets. Reflectance functions in both the cross and machine

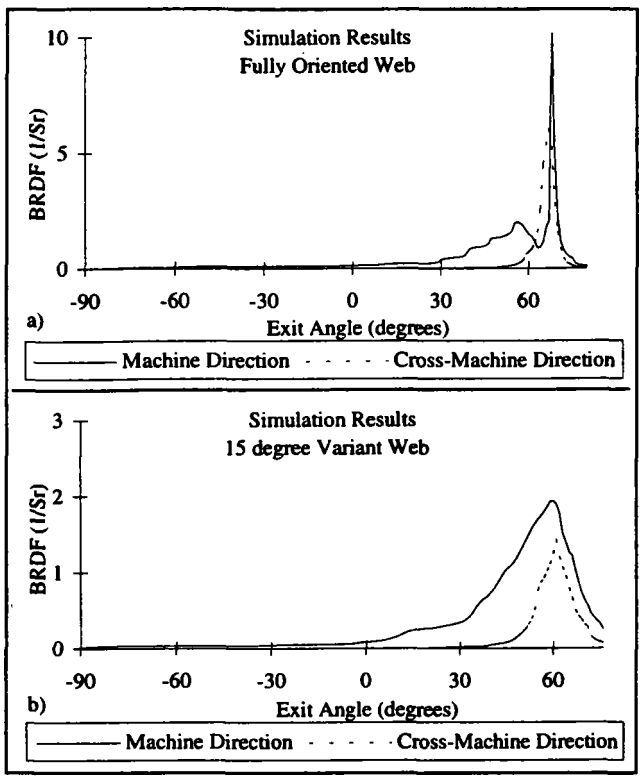

Figure 10a and 10b: Simulation results for a fully oriented sheet model and a 15° variant web at -75° incident illumination.

direction were generated using these models and are shown in Figure 10.

As seen in figure 10a, the specular peak in the cross-machine direction of the fully oriented case is smaller than the corresponding peak in the machine direction. The characteristics of these curves are similar in nature to the measurement results shown in Figure 9. The 15° variant model more realistically models the orientation that would be found in an actual sheet, and these results are shown in Figure 10b. There is still a significant anisotropy exhibited in the reflectance functions of this model. Figure 10c shows the results of simulations on the fully random model. These results confirm that the anisotropic effects disappear for a web that has fibers oriented in an entirely random fashion.

While the anisotropic reflective properties of a sheet could be inferred from its method of manufacture, the existence of retroreflectance was initially a surprise. This effect was discovered only after examining the results from the first set of measurements. Backscatter, or enhanced retroreflectance, has in fact been previously reported for a number of a materials (Oetking 1966, Egan and Hilgeman 1975, and Kuga and Ishimaru

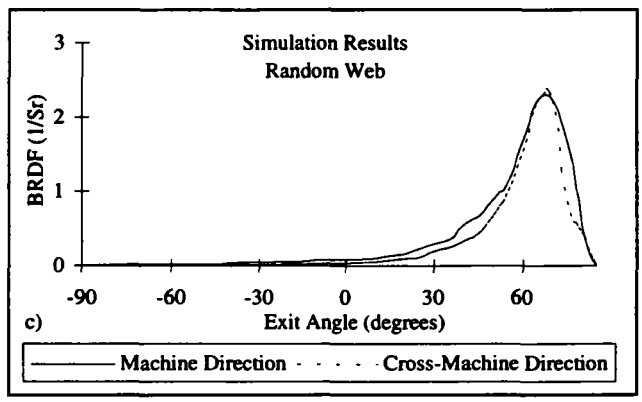

Figure 10c: Simulation results for a fully random web shown at -75° incident illumination.

1984, Mendez and O'Donnell 1987). In the case of the manufactured sheet, it was theorized that the geometry of the coating contributed to the retroreflectance. The paper geometries modeled up to this point had not produced reflectance functions that contained retroreflection peaks. The main difference between these models and the actual manufactured sheet was the addition of a coating. The aspect of a coating that has the most influence on the spatial distribution of scattered light is the shape of the particles used in the coating.

Clay and calcium carbonate are the two primary components of the coating mixture used in the manufactured specimen. The platelet-like structure of clay tends to enhance the specular reflection of the scattered light (Clark and Ramsay, 1965). Calcium carbonate is more spheroidally shaped, and thus tends to scatter light in all directions. The spherical geometry of calcium carbonate may also contribute to the observed backscatter in the reflectance functions of the manufactured specimen. A virtual model of calcium carbonate was constructed to explore this line of reasoning.

This model consisted of a volume filled with small transparent spheres. These spheres had a radius of 500 *um*, and their index of refraction was set to be 1.6 corresponding to values reported in (Johns, 1977). The spheres were packed by a simple random insertion algorithm in a volume which measured 250 x 250 x 170 *mm*. This method is similar to the one employed by Gondek et al. (1994) to model pigmented plastics. Since the geometry of spheres will produce relatively diffuse scattering, the resulting reflectance functions showed significant amounts of energy in the retroreflection direction; but these functions were not very suggestive of the ones found in the measurement results.

A second model was developed in which the calcium carbonate coating was placed on top of a simulated base stock web. Since real coatings have a

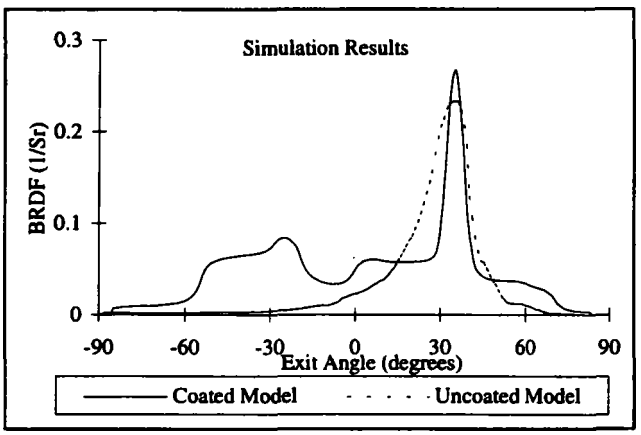

Figure 11: The effects of simulated calcium carbonate. Reflectance functions for the calcium carbonate over simulated web model and a similar web without coating.

binder applied to them in order to secure them to the substrate, the spheres in this new model were partially embedded in a medium with an index of refraction of 1.1 which represented the binder (Johns, 1977). Simulations were re-run on this second model, and the results are shown in Figure 11. These reflectance functions show similar characteristics to those of the measured sample. There is both a specular peak, and a retro-reflectance peak present in the curve. Simulations run on a similar web without the coating reveal that this effect is not present in the absence of the coatings as shown of Figure 11. The measurement results of the handmade sample also support this claim. The measured backscatter for this uncoated sample was significantly less than that of the coated sample as noted in Figure 8.

While these results support the theory that the geometry of the calcium carbonate coating contributes to the observed retro-reflectance, it must be noted that the sphere models used in these simulations represented a first order approximation of the geometry of calcium carbonate. There is reason to believe that the geometry of other materials in a sheet may also play some role in the observed backscatter phenomenon and that other optical properties might also contribute to this effect. A more precise model of both the coatings and fiber substrate would be required to conclude that the coatings are the primary source of this effect.

6 Conclusions

In this paper the technique of building local reflection models by simulating light reflection at very small scales has been applied to some difficult real world problems. Investigating the reflectance of a hummingbird feather required the use of subsurface modeling techniques that were far more complicated than those used in previous efforts to model local light reflection through simulation. The exercise showed that it was possible, by refining the subsurface model, to approach previously published analytical results. In exploring the reflectance of paper, measurements were taken using sophisticated laboratory equipment and subsurface microstructures were modeled in an attempt to match the measured reflectance properties. In this case, where there was no existing analytical expression, the model successfully captured both the anisotropic and retro-reflectance properties of the measured data. In addition, this paper extended the capabilities of the simulation tool to include refraction and multilayer interference. This is important because simulating subsurface light interactions requires a robust optics model.

All of these developments are steps along the path to creating a practical design tool for color technologists. Eventually it will be possible to simulate the reflectance properties of new surface coatings and to use computer graphic renderings to visualize their appearance. This will make it possible to go from design concept to final product without having to create a large number of prototypes. When this happens the paint and coatings industries will have the same type of computer aided design tools currently enjoyed by those in the automotive, aircraft, and electronics industries.

7 Acknowledgments

The authors wish to thank Paul Murray of Unisource Worldwide and Laurie Peterson of Potlatch Industries for providing the paper samples used in this study. The ray tracing software employed in this research was written by Jon Newman. The authors would also like to acknowledge one of the anonymous reviewers for bringing several important references to their attention.

8 References

Aho, A.V., Hopcroft, J., and Ullman, J. *The Design and Analysis of Computer Algorithms.* Addison-Wesley. Reading, Mass., 1974.

Anderson, T.F., and Richards, A. An Electron Microscope Study of Some Structural Colors of Insects. *Journal of Applied Physics.* #13, 1942, 748-758

Blinn, J.F. Models of Light Reflection for Computer Synthesized Pictures. *SIGGRAPH 94.* 1977. 192-198.

Bui-Tong, P. Illumination form Computer Generated Pictures. *Communications of the ACM.* Vol. 18. June 1975. 311-317.

Cabral, B.N. Max, N. and Springmeyer, R. Bidirectional Reflectance Functions from Surface Bump Maps. *SIGGRAPH 87.* Vol. 21 1994. 213-220.

Clark, H.B. and Ramsay, H. L. Predicting Optical Properties of Coated Papers. *Tappi* Vol. 48 #11 Nov. 1965. 609-612.

Cook, R.L and Torrance K.E. A Reflectance Model for Computer Graphics. *ACM Transaction on Graphics.* Vol. 1 1984. 7-24.

Dodson, C.T.J., and Fekih, K. The Effect of Fibre Orientation of Paper Formation. *Journal of Pulp and Paper Science* Vol. 17 #6 Nov. 1991. 203-205.

Dorsey, J. and Hanrahan, P. Modeling and Rendering of Metallic Patinas. *SIGGRAPH 96.* 1996. 387-396.

Egan, W.G., and Hilgeman, T. *Retroreflectance Measurements of Photometric Standards and Coatings.* Applied Optics. Vol. 15 #7, July 1976. 1845-1849.

Evans, R.M., *An Introduction to Color.* John Wiley & Sons, New York, New York. 1948.

Gondek, J., Meyer, G. and Newman, J. Wavelength Dependent Reflectance Functions. *SIGGRAPH 94.* 1994. 213-220.

Greenwalt, C.H. *Hummingbirds.* Doubleday. Garden City, New York, 1960.

Greenwalt, C.H., Brandt, W., and Friel, D. Iridescent Colors of Hummingbird Feathers. *Journal of the Optical Society of America.* Vol. 50 #10 Oct. 1960. 1005-1013.

Hanrahan, P. and Krueger, W. Modeling Pigmented Materials for Realistic Image Synthesis. *SIGGRAPH 93.* 165-174.

He, X.D., Torrance, K., Sillion, F. and Greenberg, D. A Comprehensive Physical Model for Light Reflection. *SIGGRAPH 91.* Vol. 25. 175-186.

Heavens, O.S. *Optical Properties of Thin Solid Films.* Academic Press. New York, New York. 1955.

Hect, E. *Optics.* 2nd Ed. Addison-Wesley Publishing. Reading Mass. 1987.

Jayme, G. and Hunger, G. Electron Microscope 2- and 3-Dimensional Classification of Fibre Bonding. *Formation and Structure of Paper Vol. 1.* William Clowes and Sons. London, G.B. 1962.135-171.

Johns, W.D. Relationships Between Crystal Structures and Physical Properties. *Physical Chemistry of Pigments in Paper Coating.* TAPPI Press. Atlanta, Georgia, 1977. 20-50.

Kajiya, J. T. The Rendering Equation. *SIGGRAPH 86.* Vol. 19. 1985. 15-29.

Kuga, Y., and Ishimaru, A. Retroreflectance From A Dense Distribution Of Spherical Particles. *Journal of the Optical Society of America.* Vol. 1, #8, August 1984. 831-835.

Lettieri, T. R., Marx, E., Song, J., and Vorburger, T. V. Light Scattering from Glossy Coatings on Paper. *Applied Optics.* Vol. 30. #30, Oct. 1991. 4439-4447.

McAlister, E.D. The Christiansen Light Filter: Its Advantages and Limitations. Smithsonian Miscellaneous Collections. #93. 1935. 1-14.

Mendez, E.R., and O'Donnell, K.A. Observation of Depolarization and Backscattering Enhancement in Light Scattering from Gaussian Random Surfaces. *Optics Communications.* Vol. 61. #2, January 1987. 91-95.

Oetking, P. Photometric Studies of Diffusely Reflecting Surfaces with Applications to the Brightness of the Moon. *Journal of Geophysical Research.* Vol. 71. #10, May 1966. 2505-2513.

Rayleigh, On an Improved Apparatus for Christiansen's Experiment. *Phil. Mag.* #20. 1885. 358-360.

Smits, B.E., and Meyer, G. Newton's Colors: Simulating Interference Phenomena in Realistic Image Synthesis. *Eurographics Workshop on Photosimulation, Realism, and Physics in Computer Graphics Conference Proceedings,* 1990, 185-194.

Westin, S.H. Arvo, J.R. and Torrance, K.E. Predicting Reflectance Functions from Complex Surfaces. *SIGGRAPH 90.* Vol. 26 1990. 255-264.

Wrist, P. E. Flow Properties of Fibrous Suspensions. *Surfaces and Coatings Related to Paper and Wood.* Marchessault and Skaar ed. Syracuse University Press. Syracuse, New York, 1967. 67-95.